

Semi-realistic nucleon-nucleon interactions with improved neutron-matter properties

H. Nakada*

*Department of Physics, Graduate School of Science, Chiba University
Yayoi-cho 1-33, Inage, Chiba 263-8522, Japan*

(Dated: November 16, 2018)

Abstract

New parameter-sets of the semi-realistic nucleon-nucleon interaction are developed, by modifying the M3Y interaction but maintaining the tensor channels and the longest-range central channels. The modification is made so as to reproduce microscopic results of neutron-matter energies, in addition to the measured binding energies of doubly magic nuclei including ^{100}Sn and the even-odd mass differences of the $Z = 50$ and $N = 82$ nuclei in the self-consistent mean-field calculations. Separation energies of the proton- or neutron-magic nuclei are shown to be in fair agreement with the experimental data. With the new parameter-sets M3Y-P6 and P7, the isotropic spin-saturated symmetric nuclear matter remains stable in the density range as wide as $\rho \lesssim 6\rho_0$, while keeping desirable results of the previous parameter-set on finite nuclei. Isotope shifts of the Pb nuclei and tensor-force effects on shell structure are discussed.

PACS numbers: 21.30.Fe, 21.60.Jz, 21.65.-f, 21.10.Dr

arXiv:1206.0794v2 [nucl-th] 16 Jan 2013

*E-mail: nakada@faculty.chiba-u.jp

I. INTRODUCTION

As exotic natures of unstable nuclei such as the new magic numbers and the neutron halos are disclosed by experiments, microscopic studies based on the nucleon-nucleon (NN) interaction become even more desired in nuclear structure physics. While the fully microscopic NN (and NNN) interaction is still too complicated to cover large volume of nuclei in the periodic table despite significant progress [1–3], the semi-realistic NN interactions have been developed [4, 5] by modifying the Michigan 3-range Yukawa (M3Y) interaction [6, 7], which was originated from Brueckner’s G -matrix at the nuclear surface and expressed by the Yukawa functions. The modification has been made so that the saturation and the spin-orbit (ls) splitting should be reproduced within the mean-field approximation (MFA). Owing to the recently developed numerical methods [8–11], self-consistent calculations in the MFA [12–14] and in the random-phase approximation (RPA) [15] have been implemented using the semi-realistic interactions. Among the advantages of the M3Y-type semi-realistic interactions is that they contain realistic tensor channels as well as correct longest-range central channels originating from the one-pion exchange, which have been pointed out to play significant roles in Z - or N -dependence of the shell structure [16, 17]. The semi-realistic interactions are suitable to investigate effects of these channels within the self-consistent MFA and RPA [5].

While the parameter-sets of the M3Y-type interactions in Refs. [4, 5, 18] were adjusted to the data on the nuclear structure, some of them have been applied to the nuclear reactions [19] and to the neutron stars [20] as well. In studying structure of the neutron stars, density-dependence of the symmetry energy is crucially important [21]. It has been pointed out that the symmetry energy at low density is significant in nuclear reactions: *e.g.* the charge-exchange reactions [19] and the multi-fragmentation processes [22]. The symmetry energy at low density may also affect the so-called pygmy dipole resonance in neutron-rich nuclei [23]. However, the symmetry energy, particularly its density-dependence, was not sufficiently reliable in the previous parameter-sets in Refs. [5, 18] as pointed out in Ref. [24], giving rise to instability of the symmetric nuclear matter at the density $\rho \gtrsim 0.6 \text{ fm}^{-3}$, which is not consistent with microscopic calculations [25]. In this article, we shall propose new parameter-sets of the M3Y-type semi-realistic NN interaction. As far as the energy of the symmetric nuclear matter is fixed, the symmetry energy at each density is well connected to the energy of the neutron matter. The new parameters are determined by fitting the neutron-matter energy to microscopic result in Ref. [26] (FP) or [25] (APR). Moreover, we additionally take into consideration the binding energy of ^{100}Sn . As argued later, the symmetry energy at the saturation point tends to be fixed with good precision by fitting the parameters both to ^{100}Sn and ^{132}Sn . The symmetry energy is thus constrained to good degree in the new parameter-sets. Corresponding to the microscopic results on the neutron-matter energy, we obtain two parameter-sets ‘M3Y-P6’ (fitted to FP) and ‘M3Y-P7’ (to APR). Although the parameters are determined from a limited number of data, they will be useful for investigating various aspects of nuclear properties, as will be illustrated by separation energies of the proton- and neutron-magic nuclei and by Z - or N -dependence of shell structure.

II. M3Y-TYPE INTERACTION

We take a non-relativistic isoscalar nuclear Hamiltonian of

$$H_N = K + V_N; \quad K = \sum_i \frac{\mathbf{p}_i^2}{2M}, \quad V_N = \sum_{i<j} v_{ij}, \quad (1)$$

with i and j representing the indices of individual nucleons. We set $M = (M_p + M_n)/2$ throughout this paper, where M_p (M_n) is the mass of a proton (a neutron) [27]. For the effective NN interaction v_{ij} , the following form is considered,

$$\begin{aligned} v_{ij} &= v_{ij}^{(C)} + v_{ij}^{(LS)} + v_{ij}^{(TN)} + v_{ij}^{(DD)}; \\ v_{ij}^{(C)} &= \sum_n (t_n^{(SE)} P_{SE} + t_n^{(TE)} P_{TE} + t_n^{(SO)} P_{SO} + t_n^{(TO)} P_{TO}) f_n^{(C)}(r_{ij}), \\ v_{ij}^{(LS)} &= \sum_n (t_n^{(LSE)} P_{TE} + t_n^{(LSO)} P_{TO}) f_n^{(LS)}(r_{ij}) \mathbf{L}_{ij} \cdot (\mathbf{s}_i + \mathbf{s}_j), \\ v_{ij}^{(TN)} &= \sum_n (t_n^{(TNE)} P_{TE} + t_n^{(TNO)} P_{TO}) f_n^{(TN)}(r_{ij}) r_{ij}^2 S_{ij}, \\ v_{ij}^{(DD)} &= (t_\rho^{(SE)} P_{SE} \cdot [\rho(\mathbf{r}_i)]^{\alpha^{(SE)}} + t_\rho^{(TE)} P_{TE} \cdot [\rho(\mathbf{r}_i)]^{\alpha^{(TE)}}) \delta(\mathbf{r}_{ij}), \end{aligned} \quad (2)$$

where \mathbf{s}_i is the spin operator of the i -th nucleon, $\mathbf{r}_{ij} = \mathbf{r}_i - \mathbf{r}_j$, $r_{ij} = |\mathbf{r}_{ij}|$, $\mathbf{p}_{ij} = (\mathbf{p}_i - \mathbf{p}_j)/2$, $\mathbf{L}_{ij} = \mathbf{r}_{ij} \times \mathbf{p}_{ij}$, and $\rho(\mathbf{r})$ denotes the nucleon density. The tensor operator is defined by $S_{ij} = 4 [3(\mathbf{s}_i \cdot \hat{\mathbf{r}}_{ij})(\mathbf{s}_j \cdot \hat{\mathbf{r}}_{ij}) - \mathbf{s}_i \cdot \mathbf{s}_j]$ with $\hat{\mathbf{r}}_{ij} = \mathbf{r}_{ij}/r_{ij}$. The projection operators on the singlet-even (SE), triplet-even (TE), singlet-odd (SO) and triplet-odd (TO) two-particle states are

$$\begin{aligned} P_{SE} &= \frac{1 - P_\sigma}{2} \frac{1 + P_\tau}{2}, & P_{TE} &= \frac{1 + P_\sigma}{2} \frac{1 - P_\tau}{2}, \\ P_{SO} &= \frac{1 - P_\sigma}{2} \frac{1 - P_\tau}{2}, & P_{TO} &= \frac{1 + P_\sigma}{2} \frac{1 + P_\tau}{2}, \end{aligned} \quad (3)$$

where P_σ (P_τ) expresses the spin (isospin) exchange operator. The Yukawa function $f_n(r) = e^{-\mu_n r}/\mu_n r$ is assumed for all channels except $v^{(DD)}$. The density-dependent contact term $v^{(DD)}$ is added in order to reproduce the saturation properties. Physically, $v^{(DD)}$ may carry effects of the NNN interaction and of the density-dependence that is dropped in the original M3Y interaction.

We start from the M3Y-Paris interaction [7], which will be denoted by M3Y-P0 in this article as in Ref. [4]. The range parameters μ_n of M3Y-P0 are maintained in any of $v^{(C)}$, $v^{(LS)}$ and $v^{(TN)}$. As in M3Y-P0, the longest-range part in $v^{(C)}$ is kept identical to the central channels of the one-pion exchange potential (OPEP), $v_{\text{OPEP}}^{(C)}$. Although the ℓs splitting plays a significant role in the nuclear shell structure, the G -matrix is known to underestimate the ℓs splitting. Even though effects beyond the MFA may cure this problem [28], we introduce an overall enhancement factor to $v^{(LS)}$ in order to describe the shell structure within the MFA. Effects of the tensor force on the single-particle (s.p.) levels could be relevant to the new magic numbers in unstable nuclei [5, 17]. We keep $v^{(TN)}$ without any modification from M3Y-P0. Because of this $v^{(TN)}$ having realistic nature, the present M3Y-type interactions are useful to investigate the tensor-force effects within the MFA and RPA, as shown in Refs. [13–15] with the previous parameter-sets. The parameters in M3Y-P6 and P7 are tabulated in Table I, together with M3Y-P0.

TABLE I: Parameters of M3Y-type interactions.

parameters		M3Y-P0	M3Y-P6	M3Y-P7
$1/\mu_1^{(C)}$	(fm)	0.25	0.25	0.25
$t_1^{(SE)}$	(MeV)	11466.	10766.	10655.
$t_1^{(TE)}$	(MeV)	13967.	8474.	9592.
$t_1^{(SO)}$	(MeV)	-1418.	-728.	11510.
$t_1^{(TO)}$	(MeV)	11345.	12453.	13507.
$1/\mu_2^{(C)}$	(fm)	0.40	0.40	0.40
$t_2^{(SE)}$	(MeV)	-3556.	-3520.	-3556.
$t_2^{(TE)}$	(MeV)	-4594.	-4594.	-4594.
$t_2^{(SO)}$	(MeV)	950.	1386.	1283.
$t_2^{(TO)}$	(MeV)	-1900.	-1588.	-1812.
$1/\mu_3^{(C)}$	(fm)	1.414	1.414	1.414
$t_3^{(SE)}$	(MeV)	-10.463	-10.463	-10.463
$t_3^{(TE)}$	(MeV)	-10.463	-10.463	-10.463
$t_3^{(SO)}$	(MeV)	31.389	31.389	31.389
$t_3^{(TO)}$	(MeV)	3.488	3.488	3.488
$1/\mu_1^{(LS)}$	(fm)	0.25	0.25	0.25
$t_1^{(LSE)}$	(MeV)	-5101.	-11222.2	-11732.3
$t_1^{(LSO)}$	(MeV)	-1897.	-4173.4	-4363.1
$1/\mu_2^{(LS)}$	(fm)	0.40	0.40	0.40
$t_2^{(LSE)}$	(MeV)	-337.	-741.4	-775.1
$t_2^{(LSO)}$	(MeV)	-632.	-1390.4	-1453.6
$1/\mu_1^{(TN)}$	(fm)	0.40	0.40	0.40
$t_1^{(TNE)}$	(MeV·fm ⁻²)	-1096.	-1096.	-1096.
$t_1^{(TNO)}$	(MeV·fm ⁻²)	244.	244.	244.
$1/\mu_2^{(TN)}$	(fm)	0.70	0.70	0.70
$t_2^{(TNE)}$	(MeV·fm ⁻²)	-30.9	-30.9	-30.9
$t_2^{(TNO)}$	(MeV·fm ⁻²)	15.6	15.6	15.6
$\alpha^{(SE)}$		—	1	1
$t_\rho^{(SE)}$	(MeV·fm ³)	0.	384.	830.
$\alpha^{(TE)}$		—	1/3	1/3
$t_\rho^{(TE)}$	(MeV·fm)	0.	1930.	1478.

III. PROPERTIES OF NUCLEAR MATTER

We first apply the new semi-realistic interactions to the infinite nuclear matter in the Hartree-Fock (HF) approximation. Notice that only $v^{(C)} + v^{(DD)}$ in Eq. (2) contributes to the nuclear matter properties in the MFA. Energy of the nuclear matter is a function of the

following variables,

$$\begin{aligned}
\rho &= \sum_{\sigma\tau} \rho_{\tau\sigma}, \\
\eta_s &= \frac{\sum_{\sigma\tau} \sigma \rho_{\tau\sigma}}{\rho} = \frac{\rho_{p\uparrow} - \rho_{p\downarrow} + \rho_{n\uparrow} - \rho_{n\downarrow}}{\rho}, \\
\eta_t &= \frac{\sum_{\sigma\tau} \tau \rho_{\tau\sigma}}{\rho} = \frac{\rho_{p\uparrow} + \rho_{p\downarrow} - \rho_{n\uparrow} - \rho_{n\downarrow}}{\rho}, \\
\eta_{st} &= \frac{\sum_{\sigma\tau} \sigma\tau \rho_{\tau\sigma}}{\rho} = \frac{\rho_{p\uparrow} - \rho_{p\downarrow} - \rho_{n\uparrow} + \rho_{n\downarrow}}{\rho},
\end{aligned} \tag{4}$$

where $\tau = p, n$ and $\sigma = \uparrow, \downarrow$ are sometimes substituted by ± 1 without confusion. As we restrict ourselves to the properties at zero temperature, the density depending on the spin and the isospin $\rho_{\tau\sigma}$ is related to the Fermi momentum $k_{F\tau\sigma}$ via

$$\rho_{\tau\sigma} = \frac{1}{6\pi^2} k_{F\tau\sigma}^3. \tag{5}$$

Basic formulas to calculate the nuclear matter energy and its derivatives for given $k_{F\tau\sigma}$ were derived in Ref. [4]. Note that the superfluidity barely influences the nuclear matter energy, even if it takes place.

We shall denote energy per nucleon (E/A) by \mathcal{E} , where E is the expectation value of H_N for the nuclear matter. The spin-saturated symmetric matter is characterized by $\eta_s = \eta_t = \eta_{st} = 0$, for which we represent $k_{F\tau\sigma}$ simply by k_F . Minimization of $\mathcal{E}(\rho)$,

$$\left. \frac{\partial \mathcal{E}}{\partial \rho} \right|_0 = \left. \frac{\partial \mathcal{E}}{\partial k_F} \right|_0 = 0, \tag{6}$$

determines the saturation density ρ_0 (equivalently, k_{F0}) and the saturation energy \mathcal{E}_0 . The expression $|_0$ indicates evaluation at the saturation point.

We depict $\mathcal{E}(\rho)$ for the spin-saturated symmetric nuclear matter in Fig. 1, up to $\rho \approx 5\rho_0$. The results of the new semi-realistic (*i.e.* M3Y-P6 and P7) interactions are compared with those of the Skyrme SLy5 [29], the Gogny D1S [30] and D1M [31] interactions. While all effective interactions give close $\mathcal{E}(\rho)$ at $\rho \lesssim \rho_0$, interaction-dependence is visible at $\rho \gtrsim 2\rho_0$, though the SLy5 energy almost coincides with the M3Y-P6 one.

Energy per nucleon in the spin-saturated neutron matter (*i.e.* $\eta_t = -1$, $\eta_s = \eta_{st} = 0$) is shown in Fig. 2. The FP [26] and APR [25] results, to which M3Y-P6 and P7 are respectively fitted, are also presented. Having been fitted to a microscopic result [32] as well, the energy with SLy5 is close to that with M3Y-P7 at any ρ . The stronger ρ dependence in M3Y-P6 and P7 than in D1S and D1M originates from the choice $\alpha^{(SE)} = 1$ in $v^{(DD)}$, and enables us to reproduce the microscopic results. Since $v^{(DD)}$ drives repulsion in the SE channel at high ρ but does not in the TO channel, the interactions having the form of Eq. (2) may give rise to the spin-polarized phase at high ρ in the pure neutron matter. However, the transition to the spin-polarized phase is delayed until $\rho \approx 9\rho_0$ ($20\rho_0$) for M3Y-P7 (P6), almost irrelevant even to the neutron stars.

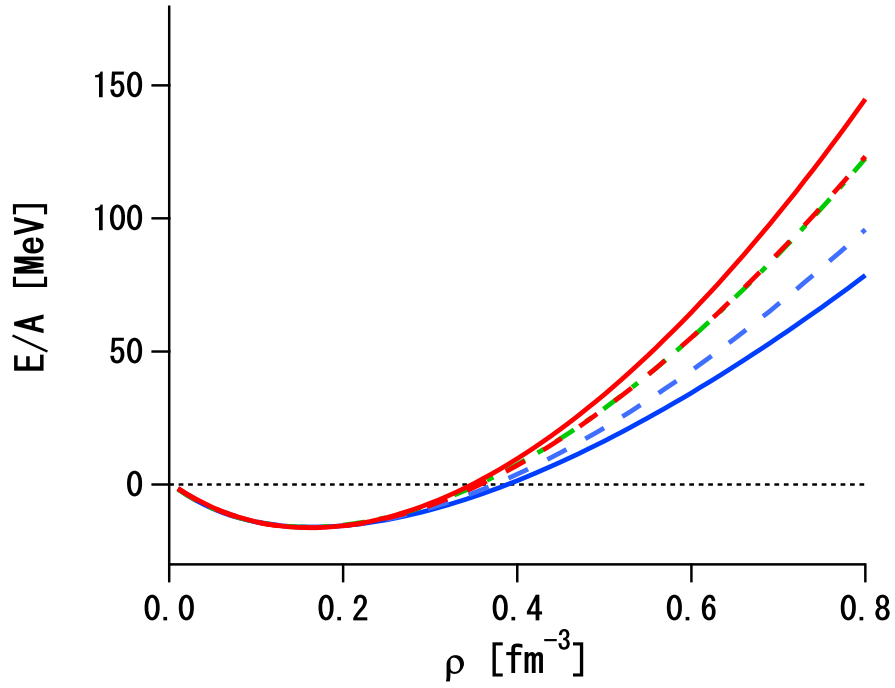


FIG. 1: (Color online) $\mathcal{E} = E/A$ vs. ρ in the symmetric nuclear matter, calculated with M3Y-P6 (red dashed line), M3Y-P7 (red solid line), D1S (blue solid line), D1M (blue dashed line) and SLy5 (green dot-dashed line).

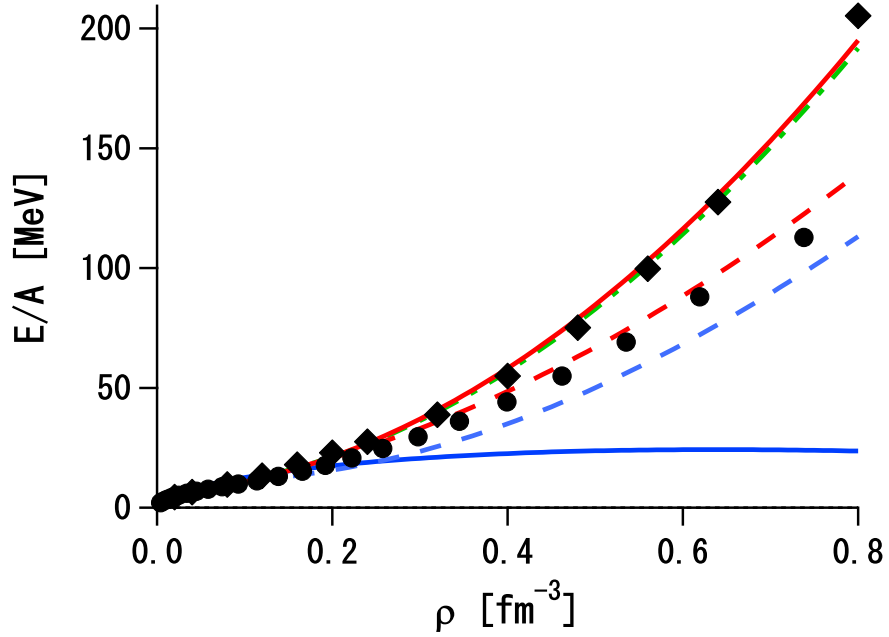


FIG. 2: (Color online) $\mathcal{E} = E/A$ vs. ρ in the pure neutron matter. Circles and diamonds represent the FP and APR results, respectively. See Fig. 1 for the other conventions.

TABLE II: Nuclear matter properties at the saturation point.

	M3Y-P6	M3Y-P7	D1S	D1M	SLy5
k_{F0} (fm ⁻¹)	1.340	1.340	1.342	1.346	1.334
\mathcal{E}_0 (MeV)	-16.24	-16.22	-16.01	-16.02	-15.98
\mathcal{K}_0 (MeV)	239.7	254.7	202.9	225.0	229.9
M_0^*/M	0.596	0.589	0.697	0.746	0.697
a_{t0} (MeV)	32.14	31.74	31.12	28.55	32.03
a_{s0} (MeV)	26.47	23.04	26.18	16.56	37.47
a_{st0} (MeV)	41.00	43.30	29.13	28.71	15.15
\mathcal{Q}_0 (MeV)	-378.0	-320.1	-515.7	-459.0	-363.9
\mathcal{L}_{t0} (MeV)	44.64	51.53	22.44	24.83	48.27

The symmetry energy is defined by the second derivative of \mathcal{E} with respect to η_t for the spin-saturated matter,

$$a_t(\rho) = \left. \frac{1}{2} \frac{\partial^2 \mathcal{E}}{\partial \eta_t^2} \right|_{\rho}. \quad (7)$$

Here $|_{\rho}$ indicates $\eta_t = \eta_s = \eta_{st} = 0$ but ρ left as a variable. The symmetry energy at the saturation point $a_t(\rho_0)$ is denoted by a_{t0} . Analogously, we define

$$a_s(\rho) = \left. \frac{1}{2} \frac{\partial^2 \mathcal{E}}{\partial \eta_s^2} \right|_{\rho}, \quad a_{st}(\rho) = \left. \frac{1}{2} \frac{\partial^2 \mathcal{E}}{\partial \eta_{st}^2} \right|_{\rho}, \quad (8)$$

and $a_{s0} = a_s(\rho_0)$, $a_{st0} = a_{st}(\rho_0)$. The incompressibility at the saturation point is obtained by

$$\mathcal{K}_0 = k_F^2 \left. \frac{\partial^2 \mathcal{E}}{\partial k_F^2} \right|_0 = 9\rho^2 \left. \frac{\partial^2 \mathcal{E}}{\partial \rho^2} \right|_0. \quad (9)$$

The effective mass (k -mass) is defined by a derivative of the s.p. energy $\varepsilon(\mathbf{k}\sigma\tau)$. We denote the effective mass at the saturation point by M_0^* , which is given as

$$\left. \frac{\partial \varepsilon(\mathbf{k}\sigma\tau)}{\partial k} \right|_0 = \frac{k_{F0}}{M_0^*}. \quad (10)$$

These characteristic quantities calculated from the new semi-realistic interactions are tabulated in Tables II. Those from D1S, D1M and SLy5 are also displayed for comparison. Also compare them with the empirical values $k_{F0} \sim 1.33 - 1.34 \text{ fm}^{-1}$, $\mathcal{E}_0 \sim -16 \text{ MeV}$, $\mathcal{K} \sim 240 \text{ MeV}$ [33] and $a_{t0} \sim 30 \text{ MeV}$ [34]. It is remarked that the fit both to ¹⁰⁰Sn and ¹³²Sn (see Table IV) well constrains a_{t0} in the M3Y-type interactions with good precision, to $a_{t0} \approx 32 \text{ MeV}$. This a_{t0} value is in harmony with a_{t0} of SLy5, though not so with a_{t0} of D1M and of a recently proposed Skyrme-type energy density functional UNDEF1 [35]. The effective mass ($M_0^* \approx 0.6 M$) of the current M3Y-type interactions is not much changeable, which does not contradict to a microscopic result [36] but is lower than the value that reproduces collective excitations in the RPA (*e.g.* the D1M value).

As mentioned in Introduction, ρ -dependence of the symmetry energy attracts interest. The first derivative of $a_t(\rho)$ at ρ_0 is under debate, which is parametrized as

$$\mathcal{L}_{t0} = 3 \left. \frac{d}{d\rho} a_t(\rho) \right|_0 = \frac{1}{2} k_F \left. \frac{\partial^3 \mathcal{E}}{\partial k_F \partial \eta_t^2} \right|_0 = \frac{3}{2} \rho \left. \frac{\partial^3 \mathcal{E}}{\partial \rho \partial \eta_t^2} \right|_0. \quad (11)$$

The characteristic coefficient \mathcal{L}_{t0} , along with the third derivative of \mathcal{E} with respect to ρ that is denoted by \mathcal{Q}_0 ,

$$\mathcal{Q}_0 = k_F^3 \left. \frac{\partial^3 \mathcal{E}}{\partial k_F^3} \right|_0 = 27 \rho^3 \left. \frac{\partial^3 \mathcal{E}}{\partial \rho^3} \right|_0, \quad (12)$$

are also presented in Table II. It is noteworthy that M3Y-P6 and P7 have higher \mathcal{L}_{t0} than D1S and D1M, in contrast to the previous parameter-set M3Y-P5 [5] that has comparable \mathcal{L}_{t0} to D1S and D1M. The higher \mathcal{L}_{t0} values seem favorable for describing the low-lying $E1$ strengths [23].

The symmetry energy $a_t(\rho)$ in a wider region of ρ is depicted in Fig. 3, along with $a_s(\rho)$ and $a_{st}(\rho)$. If any of $a_t(\rho)$, $a_s(\rho)$ or $a_{st}(\rho)$ is negative, the spin-saturated symmetric nuclear matter becomes unstable, undergoing phase transition. With D1S the symmetric matter is unstable beyond $\rho \approx 3.4\rho_0$, as inferred from Fig. 2 and manifested in Fig. 3-a). Moreover, Fig. 3-c) implies that the magnetized phase emerges at moderately high ρ , when we employ SLy5 or D1M. The transition takes place at $\rho \approx 2.1\rho_0$ ($3.0\rho_0$) in the SLy5 (D1M) result. Similar instability occurs at $\rho \approx (1.2 - 3)\rho_0$ for most available parameter-sets of the Skyrme interaction including the tensor channels, even if deformation of the Fermi sphere is ignored [37]. On the contrary, in this density region the isotropic nuclear matter is stable against spin or isospin asymmetry under M3Y-P6 and P7, though M3Y-P6 gives decreasing $a_t(\rho)$ in $\rho > 2.2\rho_0$, which eventually becomes negative in $\rho > 5.8\rho_0$.

The Landau-Migdal (LM) parameters have been used to argue global characters of excitation modes of nuclei. Employing the analytic formulas given in Ref. [4], we evaluate the LM parameters at the saturation point for the new semi-realistic interactions, as shown in Table III. See Ref. [4] for definition of the LM parameters. Several LM parameters are related to the characteristic coefficients in Table II as follows,

$$\begin{aligned} \frac{M_0^*}{M} &= 1 + \frac{1}{3} f_1, & \mathcal{K}_0 &= \frac{3k_{F0}^2}{M_0^*} (1 + f_0), & a_{t0} &= \frac{k_{F0}^2}{6M_0^*} (1 + f'_0), \\ a_{s0} &= \frac{k_{F0}^2}{6M_0^*} (1 + g_0), & a_{st0} &= \frac{k_{F0}^2}{6M_0^*} (1 + g'_0). \end{aligned} \quad (13)$$

It has been known that g_0 is small while g'_0 is relatively large (≈ 1) [38]. M3Y-P6 and P7 hold reasonable characters on the spin and isospin channels as the previous parameters, owing significantly to $v_{\text{OPEP}}^{(C)}$ [4].

IV. APPLICATIONS TO FINITE NUCLEI

We next apply the new semi-realistic interactions to finite nuclei within the MFA. The Hamiltonian $H = H_N + V_C - H_{\text{c.m.}}$ is used, with H_N given in Eq. (1). V_C and $H_{\text{c.m.}}$ represent the Coulomb interaction and the center-of-mass (c.m.) Hamiltonian. We have made no additional approximation on H , by handling the exchange term of V_C and the two-body terms of $H_{\text{c.m.}}$ explicitly. Effects of V_C on the proton pairing, which have recently

TABLE III: Landau-Migdal parameters at the saturation point.

	M3Y-P6	M3Y-P7	D1S	D1M	SLy5
f_0	-0.360	-0.329	-0.369	-0.255	-0.276
f_1	-1.211	-1.233	-0.909	-0.762	-0.909
f_2	-0.394	-0.381	-0.558	-0.302	0.0
f_3	-0.183	-0.177	-0.157	-0.058	0.0
f'_0	0.544	0.506	0.743	0.701	0.815
f'_1	0.511	0.571	0.470	0.378	-0.387
f'_2	0.225	0.234	0.342	0.632	0.0
f'_3	0.090	0.091	0.100	0.137	0.0
g_0	0.272	0.093	0.466	-0.013	1.123
g_1	0.231	0.337	-0.184	-0.380	0.253
g_2	0.163	0.179	0.245	0.483	0.0
g_3	0.077	0.079	0.091	0.114	0.0
g'_0	0.970	1.055	0.631	0.711	-0.141
g'_1	0.157	0.069	0.610	0.652	1.043
g'_2	0.053	0.044	-0.038	-0.243	0.0
g'_3	0.004	0.004	-0.036	-0.064	0.0

been recognized to be sizable [39], are explicitly included in the Hartree-Fock-Bogolyubov (HFB) calculations as well.

The algorithm based on the Gaussian expansion method (GEM) [8, 9] is applied for all the numerical calculations of finite nuclei in this article. In this method we employ the s.p. basis-functions of

$$\varphi_{\nu\ell jm}(\mathbf{r}) = R_{\nu\ell j}(r)[Y^{(\ell)}(\hat{\mathbf{r}})\chi_{\sigma}]_m^{(j)}; \quad R_{\nu\ell j}(r) = \mathcal{N}_{\nu\ell j} r^{\ell} \exp(-\nu r^2), \quad (14)$$

apart from the isospin index, where $Y^{(\ell)}(\hat{\mathbf{r}})$ is the spherical harmonics and χ_{σ} the spin wave function. For the range parameter ν , which is generally a complex number ($\nu = \nu_r + i\nu_i$), we adopt the following values [10]:

$$\nu_r = \nu_0 b^{-2n}, \quad \begin{cases} \nu_i = 0 & (n = 0, 1, \dots, 5) \\ \frac{\nu_i}{\nu_r} = \pm \frac{\pi}{2} & (n = 0, 1, 2) \end{cases}, \quad (15)$$

with $\nu_0 = (2.40 \text{ fm})^{-2}$ and $b = 1.25$, resulting in 12 bases for each (ℓ, j) . In the HFB calculations the s.p. space is truncated as $\ell \leq 8$ (for the $Z = 82$ and $N = 126$ nuclei) or $\ell \leq 7$ (for the lighter ones). As shown in Ref. [10], the above set of the GEM bases can cover wide range of nuclear mass with good precision.

In the following we shall show results of the spherical HF and HFB calculations using the new M3Y-P6 and P7 interactions, in comparison with those using the Gogny D1S and D1M interactions. Although there have been more advanced calculations using the Gogny interactions, *e.g.* the calculations based on the generator-coordinate method [40], comparison is made only at the MFA level in this paper, leaving extensive applications of the M3Y-type interactions as a future work.

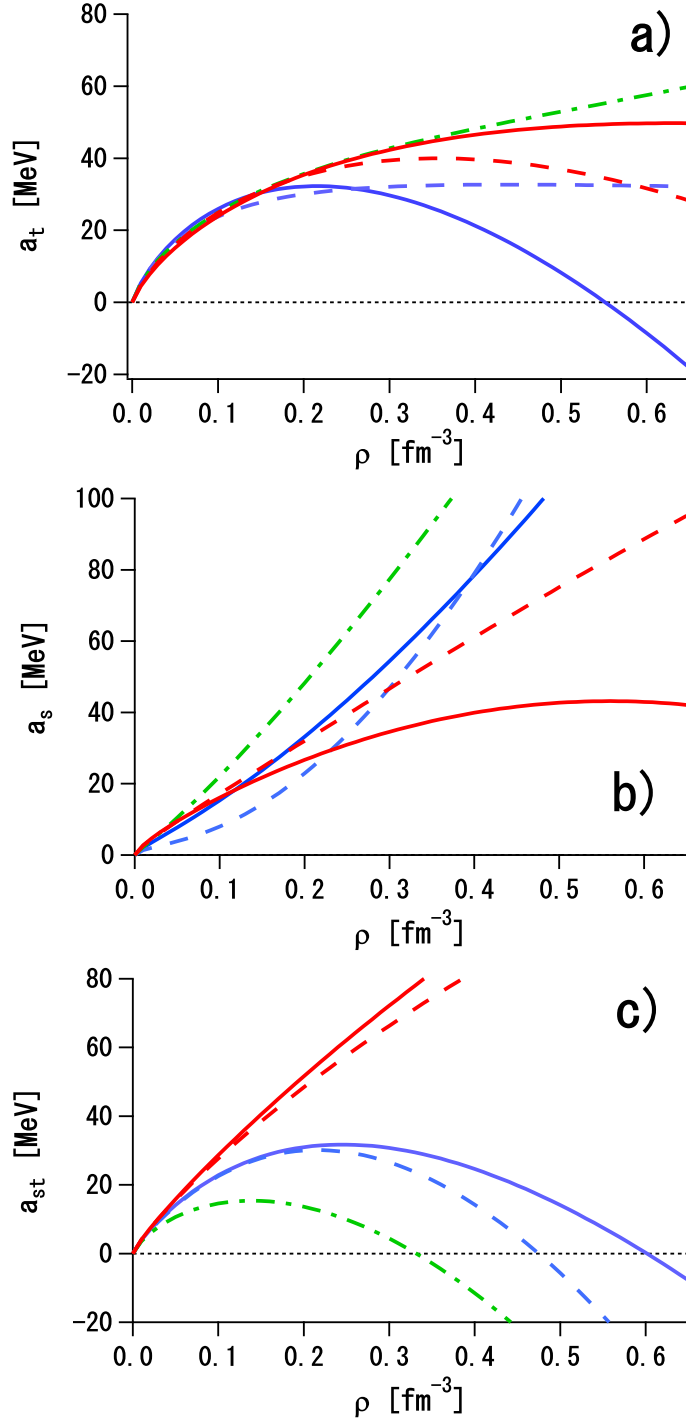


FIG. 3: (Color online) a) $a_t(\rho)$, b) $a_s(\rho)$ and c) $a_{st}(\rho)$ in the symmetric nuclear matter. See Fig. 1 for the conventions.

TABLE IV: Binding energies ($-E$) and rms matter radii ($\sqrt{\langle r^2 \rangle}$) of several doubly magic nuclei. Experimental data are taken from Refs. [41–44].

		Exp.	M3Y-P6	M3Y-P7	D1S	D1M
^{16}O	$-E$ (MeV)	127.6	126.3	125.9	129.5	128.2
	$\sqrt{\langle r^2 \rangle}$ (fm)	2.61	2.59	2.57	2.61	2.57
^{24}O	$-E$ (MeV)	168.5	166.2	167.4	168.6	167.3
	$\sqrt{\langle r^2 \rangle}$ (fm)	3.19	3.05	3.03	3.01	2.98
^{40}Ca	$-E$ (MeV)	342.1	335.9	334.3	344.6	342.2
	$\sqrt{\langle r^2 \rangle}$ (fm)	3.47	3.37	3.35	3.37	3.33
^{48}Ca	$-E$ (MeV)	416.0	413.8	414.9	416.8	414.6
	$\sqrt{\langle r^2 \rangle}$ (fm)	3.57	3.51	3.49	3.51	3.48
^{90}Zr	$-E$ (MeV)	783.9	781.1	780.8	785.9	782.1
	$\sqrt{\langle r^2 \rangle}$ (fm)	4.32	4.23	4.22	4.24	4.20
^{100}Sn	$-E$ (MeV)	824.8	822.5	822.8	831.6	824.9
	$\sqrt{\langle r^2 \rangle}$ (fm)	—	4.36	4.34	4.36	4.32
^{132}Sn	$-E$ (MeV)	1102.9	1097.8	1100.8	1104.1	1104.5
	$\sqrt{\langle r^2 \rangle}$ (fm)	—	4.78	4.77	4.77	4.72
^{208}Pb	$-E$ (MeV)	1636.4	1634.5	1635.5	1639.0	1638.9
	$\sqrt{\langle r^2 \rangle}$ (fm)	5.49	5.53	5.51	5.51	5.47

A. Doubly magic nuclei

The spherical HF approach is rationally expected to be a good approximation for the ground states of the doubly magic nuclei. We present the binding energies and the rms matter radii of several doubly magic nuclei in Table IV. The spherical HF results using the new semi-realistic interactions are compared with those using D1S and D1M, as well as with the experimental data. Influence of the c.m. motion on the matter radii is subtracted in a similar manner to the c.m. energies [4]. The binding energies of these nuclei by the M3Y-P6 and P7 interactions are in agreement with the measured values within 5 MeV accuracy, except ^{40}Ca . This accuracy is comparable to those of D1S and D1M. In ^{40}Ca , influence of octupole correlations might be strong, as suggested by the low 3_1^- energy in measurements [45] and mentioned in Ref. [5]. For this reason we have not taken this discrepancy seriously at the present stage, while future study is needed on this problem. The rms matter radii of these nuclei calculated from M3Y-P6 and P7 are also in fair agreement with the data. We point out that D1S has not predicted accurate energy of ^{100}Sn , and that D1M systematically gives smaller radii than the measured ones.

The non-central channels of the effective interaction, $v^{(\text{LS})}$ and $v^{(\text{TN})}$, are responsible for the ℓs splitting of the s.p. levels and its nucleus-dependence. We display the s.p. levels of ^{208}Pb calculated in the HF approximation, comparing to the observed levels in Fig. 4. The experimental s.p. levels are taken from the lowest states having specific spin-parity in the $A = 207$ or 209 nuclei. Because of the fragmentation via the coupling to the many-particle-many-hole configurations, these observed states do not straightforwardly correspond to the s.p. levels in the MFA. In M3Y-P6 and P7 the non-central channels are not changed from

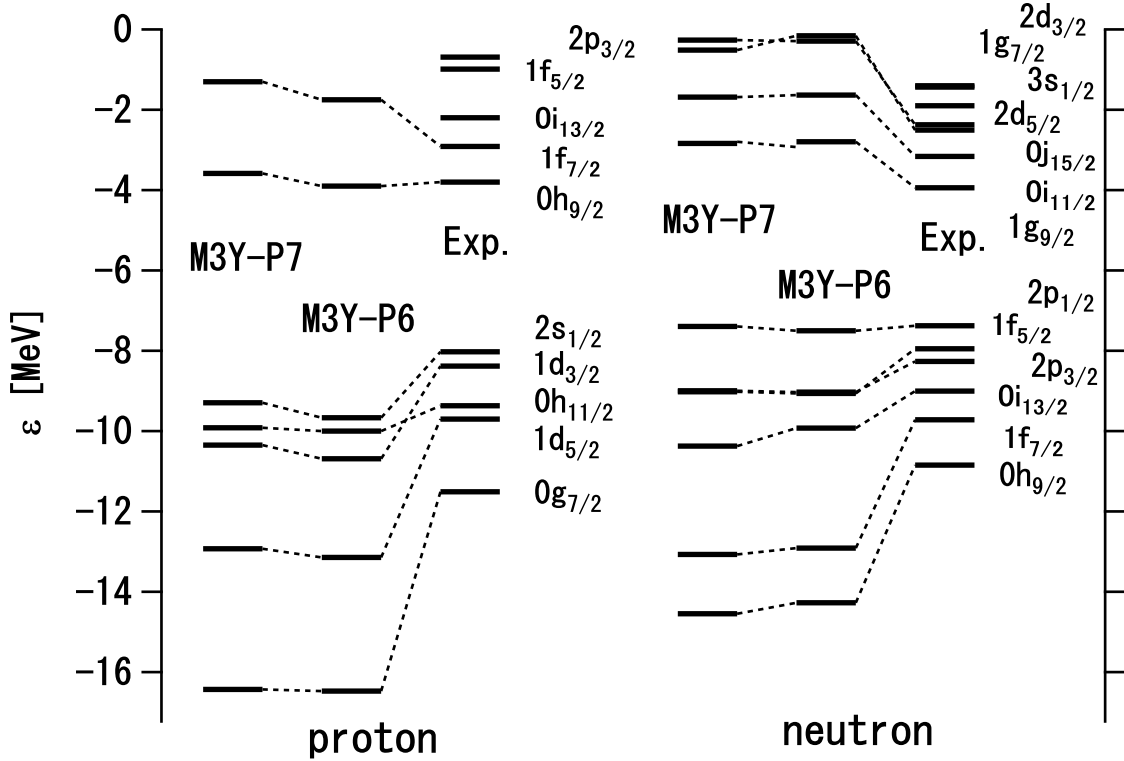


FIG. 4: Single-particle energies for ^{208}Pb . Experimental values are extracted from Refs. [41, 45].

TABLE V: Difference between proton and neutron rms radii $\sqrt{\langle r^2 \rangle_n} - \sqrt{\langle r^2 \rangle_p}$ in ^{208}Pb (fm) by the HF calculations with several interactions.

M3Y-P6	M3Y-P7	D1S	D1M
0.158	0.161	0.136	0.112

M3Y-P0 except the overall enhancement factor to $v^{(\text{LS})}$. This factor is determined so that the level ordering should not differ seriously from the observed one around ^{208}Pb . While appropriateness of the enhancement factor to $v^{(\text{LS})}$ should further be investigated in future studies, it is a simple and useful cure to the ls splitting.

It has been recognized that the neutron-skin thickness in ^{208}Pb is connected to the ρ dependence of the symmetry energy [46], particularly the \mathcal{L}_{t0} parameter. Table V presents difference between proton and neutron rms radii $\sqrt{\langle r^2 \rangle_n} - \sqrt{\langle r^2 \rangle_p}$ in ^{208}Pb . The values of M3Y-P6 and P7 are in good agreement with the recent experimental value drawn from the $E1$ strengths [47].

B. Proton- or neutron-magic nuclei

The spherical HFB approach provides us with a reasonable approximation for the nuclei in which Z or N is a magic number. The odd- Z or N nuclei can be handled in the equal-

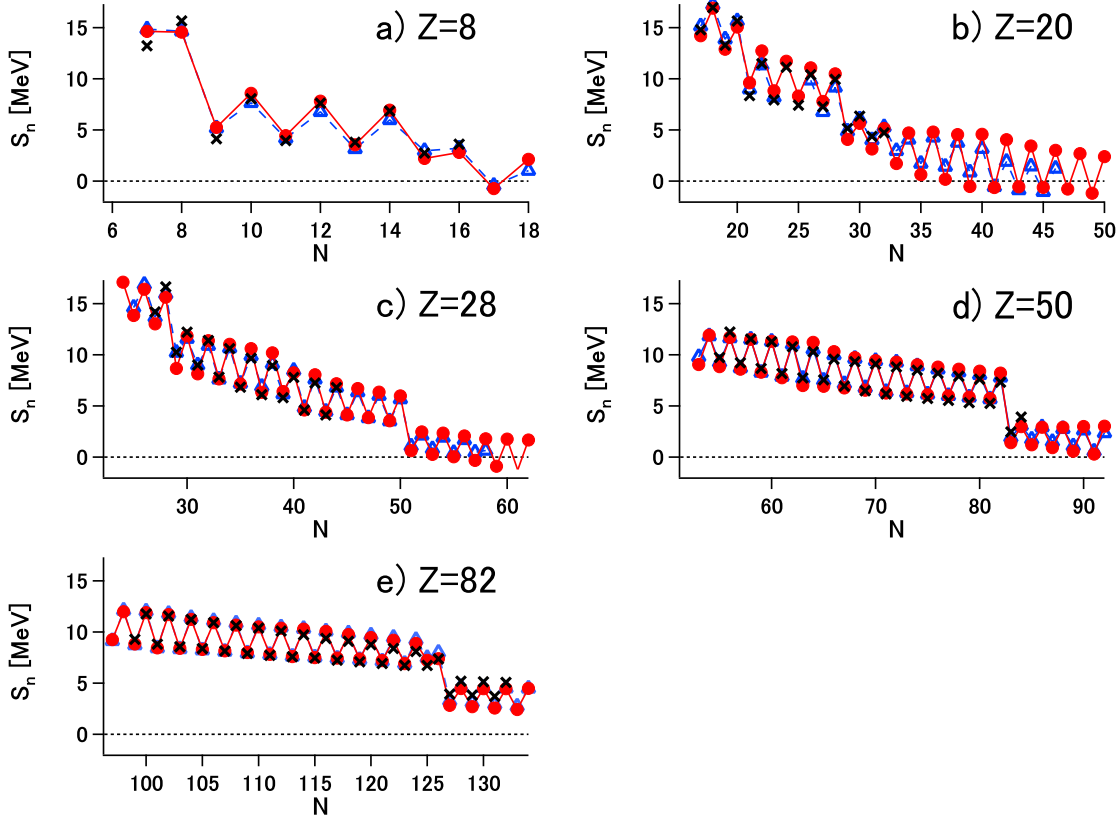


FIG. 5: (Color online) Neutron separation energies for a) $Z = 8$, b) $Z = 20$, c) $Z = 28$, d) $Z = 50$ and e) $Z = 82$ nuclei, calculated with M3Y-P7 (red circles) and D1M (blue open triangles). Lines are drawn to guide eyes. Experimental values are taken from Ref. [41] and presented by the crosses.

filling approximation [48, 49]. In fixing the new parameter-sets, we have taken into account the pairing properties by fitting to the data on the even-odd mass differences in the $Z = 50$, $N \sim 70$ and the $N = 82$, $Z \sim 60$ nuclei [50].

In Fig. 5 (Fig. 6), the neutron (proton) separation energies S_n (S_p) are plotted for the $Z = \text{magic}$ ($N = \text{magic}$) nuclei. The S_n and S_p values of M3Y-P6, which are always close to those of M3Y-P7, are not presented. Similarly, being close to the D1M ones, the D1S results are not displayed. Notice that the even-odd mass difference is proportional to the difference of the separation energies between the adjacent nuclei, while the two-neutron (two-proton) separation energy is the sum of S_n 's (S_p 's) of the two neighboring nuclei. Although there are certain discrepancies if we look into their details, M3Y-P6 and P7 give separation energies in agreement with the measured ones with the accuracy similar to D1S and D1M.

It has been suggested that isotope shifts of the Pb nuclei may be relevant to the ℓs potential [51], which is primarily determined by $v^{(LS)}$. In $\delta\sqrt{\langle r^2 \rangle_p}(^{A}\text{Pb}) = \sqrt{\langle r^2 \rangle_p}(^{A}\text{Pb}) - \sqrt{\langle r^2 \rangle_p}(^{208}\text{Pb})$, a kink has been observed at ^{208}Pb . The zero-range LS force contained in the Gogny as well as the original Skyrme interactions operates only on the $T = 1$ two-nucleon states. It was argued that this isospin character of the LS force could be insufficient to describe the rapid rise of $\delta\sqrt{\langle r^2 \rangle_p}$ in $N > 126$. Having $v^{(LS)}$ with finite ranges that acts also on the $T = 0$ channel, it may be interesting whether the M3Y-type interactions reproduce

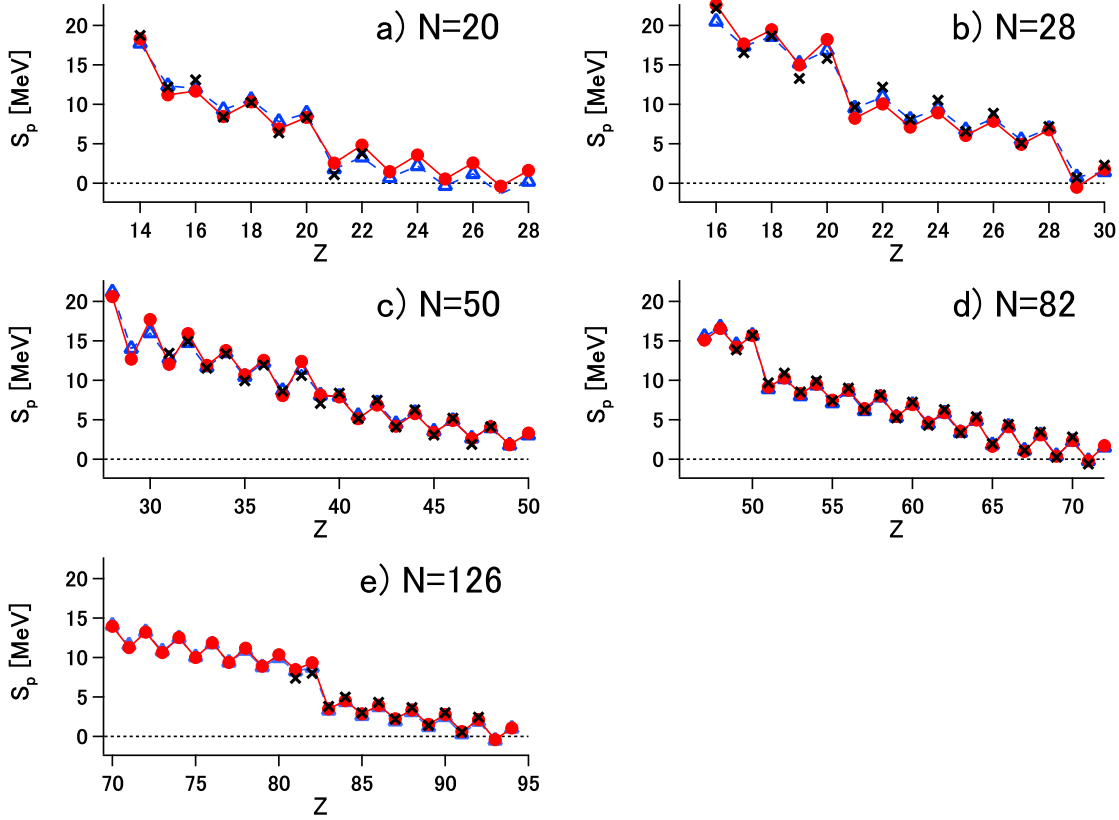


FIG. 6: (Color online) Proton separation energies for a) $N = 20$, b) $N = 28$, c) $N = 50$, d) $N = 82$ and e) $N = 126$ nuclei. See Fig. 5 for the conventions.

the kink of $\delta\sqrt{\langle r^2 \rangle}_p$.

In Fig. 7, we depict $\delta\sqrt{\langle r^2 \rangle}_p(^A\text{Pb})$ obtained by the spherical HFB calculations with M3Y-P7, D1S and D1M, in comparison with experimental data [52, 53]. The results of M3Y-P6 are almost indistinguishable from those of D1M in $N < 126$ and from those of M3Y-P7 in $N > 126$. The D1S interaction does not give clear bending at ^{208}Pb . On the contrary, although its LS force holds the zero-range form, D1M provides a visible kink at ^{208}Pb . M3Y-P7, in which $v^{(\text{LS})}$ has finite ranges, further improves $\delta\sqrt{\langle r^2 \rangle}_p$. We have confirmed that this tendency well correlates to the occupation probability on $n0i_{11/2}$, as pointed out in Ref. [54]. It seems reasonable to consider that the s.p. energy difference $\varepsilon(n0i_{11/2}) - \varepsilon(n1g_{9/2})$ is responsible for the interaction-dependence of $\delta\sqrt{\langle r^2 \rangle}_p$ in $N > 126$. However, whereas isospin character of $v^{(\text{LS})}$ plays a certain role in the s.p. energy difference, it is not yet obvious whether and how interplay of other channels, *e.g.* $v^{(\text{TN})}$ and the pairing, contributes to $\delta\sqrt{\langle r^2 \rangle}_p$.

In earlier studies [51, 54], the MFA results were compared with the data given in, *e.g.*, Ref. [52]. The kink at ^{208}Pb becomes stronger in the new data [53] because of larger values of $\delta\sqrt{\langle r^2 \rangle}_p$ in $N > 126$, which has not been reproduced within the MFA, to the author's best knowledge.

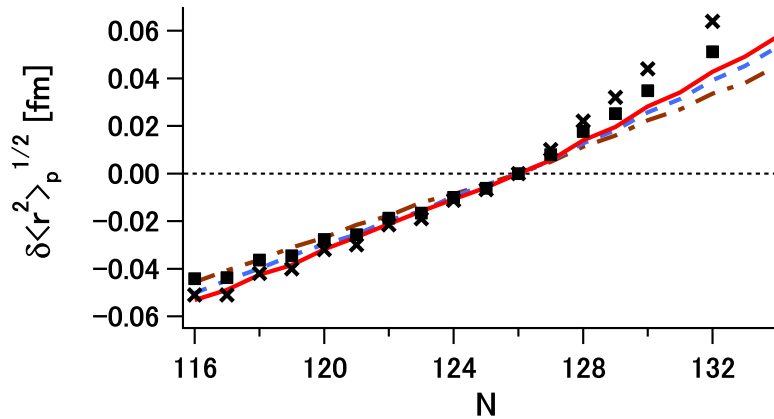


FIG. 7: (Color online) Isotope shifts of the Pb nuclei $\delta\sqrt{\langle r^2 \rangle_p}(^A\text{Pb})$, obtained from the HFB calculations with M3Y-P7 (red solid line), D1M (blue dashed line) and D1S (brown dot-dashed line). Experimental data are taken from Refs. [52] and [53], which are represented by squares and crosses, respectively.

C. Shell structure and tensor force

It has been established that the shell structure depends on the effective NN interaction of the MFA. In particular, the effects of the tensor force are significant, as clarified in the proton- or neutron-magic nuclei [5, 17]. In some nuclei the spin-isospin channels of the central force could also have appreciable effects [5, 16]. Having realistic $v^{(\text{TN})}$ and $v_{\text{OPEP}}^{(\text{C})}$, M3Y-P6 and P7 are suitable to investigating those effects as the previous interaction M3Y-P5 [5, 18]. This is a clear advantage of these semi-realistic interactions over the phenomenological interactions such as D1S and D1M. Although the results of M3Y-P6 and P7 on the shell structure are not essentially different from those of the previous parameter-set shown in Refs. [5, 14, 18], we briefly mention several notable points.

The N -dependence of the differences of the observed s.p. energies $\varepsilon(p0h_{11/2}) - \varepsilon(p1d_{5/2})$ and $\varepsilon(p0g_{7/2}) - \varepsilon(p1d_{5/2})$ in the Sn isotopes are simultaneously reproduced, with $v^{(\text{TN})}$ being crucial to the former (see Fig. 14 and related arguments in Ref. [5]). In the $N = 32$ isotones $v^{(\text{TN})}$ and $v_{\text{OPEP}}^{(\text{C})}$ give rise to significant Z -dependence of $\varepsilon(n0f_{5/2}) - \varepsilon(n1p_{3/2})$ (see Fig. 13 of Ref. [5] and Fig. 3 of Ref. [14]), possibly accounting for the new magic number $N = 32$ around ^{52}Ca [55, 56]. However, despite the presence of the realistic tensor force, the semi-realistic interactions do not predict closure of $N = 34$ at ^{54}Ca (see Fig. 3 of Ref. [18]), in contrast to the shell model prediction in Ref. [57]. While semi-magic nature of $N = 40$ is indicated at ^{68}Ni with the semi-realistic interactions as with the Gogny interactions (see Fig. 4 of Ref. [18]), which seems consistent with experiments [58], it is likely for the $N = 40$ magic nature to be broken at ^{60}Ca because of $v^{(\text{TN})}$ (see Fig. 3 of Ref. [18] and Fig. 4 of Ref. [14]). It is of interest to investigate magicity of $N = 40$ toward ^{60}Ca experimentally, which could further clarify role of $v^{(\text{TN})}$. The doubly magic nature of ^{78}Ni is predicted to hold even with $v^{(\text{TN})}$, giving $E_x(2_1^+) = 3.0 - 3.5$ MeV and $B(E2; 2_1^+ \rightarrow 0_1^+) \approx 85 e^2\text{fm}^4$ in the HF+RPA. Experimental data on 2_1^+ of ^{78}Ni are awaited.

Location of the neutron drip line for the Ca and Ni nuclei could be investigated by the new experimental facilities [59] and has been argued in Ref. [14]. We tabulate the neutron

TABLE VI: Neutron numbers of the heaviest bound Ca and Ni nuclei predicted by the spherical HFB calculations with several interactions.

Isotope	M3Y-P6	M3Y-P7	D1S	D1M
Ca	50	50	44	46
Ni	60	62	58	58

drip line predicted by the spherical HFB calculations with the M3Y-type and the Gogny interactions, in Table VI.

V. SUMMARY AND OUTLOOK

We have developed new parameter-sets of the semi-realistic effective interactions to describe low energy phenomena of nuclei. They are obtained by phenomenologically modifying several parameters in the M3Y-Paris interaction, while the tensor force and the OPEP part in the central force are not changed, as before. Unlike the previous parameters, the new sets M3Y-P6 and P7 are adjusted also to the microscopic (FP and APR) results of the neutron-matter energies and to the binding energy of ^{100}Sn . We therefore attain improvement on the symmetry energy, up to its density-dependence. In contrast to instability of the spin-saturated symmetric nuclear matter in the SLy5, D1S and D1M results, neither of M3Y-P6 nor P7 predicts such phase transition in the density range of $\rho \lesssim 6\rho_0$.

The new parameter-sets M3Y-P6 and P7 have been applied to the doubly magic nuclei in the spherical HF calculations, and to the proton- or neutron-magic nuclei in the spherical HFB calculations. Fair agreement with experimental data has been demonstrated for the binding energies of the doubly magic nuclei and for the nucleon separation energies of the proton- or neutron-magic nuclei. Owing to the realistic tensor force and the OPEP central force, the Z - or N -dependence of the shell structure is well described with M3Y-P6 and P7, as with the previous set M3Y-P5. The isotope shifts of the Pb nuclei have also been argued.

Future study includes application of the semi-realistic interactions to the excitations in the RPA, as well as to deformed nuclei. Moreover, extensive applications to nuclear reactions and to the neutron stars may be within the reach, which give further test of the effective interactions and a step toward unified description of nuclear structure, reactions and neutron stars.

Acknowledgments

This work is financially supported as Grant-in-Aid for Scientific Research (C), No. 22540266, by Japan Society for the Promotion of Science, and as Grant-in-Aid for Scientific Research on Innovative Areas, No. 24105008, by The Ministry of Education, Culture, Sports, Science and Technology, Japan. Numerical calculations are performed on HITAC SR16000s at Institute of Media and Information Technology in Chiba University, Yukawa Institute for Theoretical Physics in Kyoto University, Research Institute for Information Technology in Kyushu University, Information Technology Center in University of Tokyo,

- [1] S.C. Pieper, K. Varga and R.B. Wiringa, Phys. Rev. C **66**, 044310 (2002).
- [2] P. Navrátil and B.R. Barrett, Phys. Rev. C **57**, 3119 (1998); P. Navrátil, J.P. Vary and B.R. Barrett, Phys. Rev. C **62**, 054311 (2000); R. Roth, J. Langhammer, A. Calci, S. Binder and P. Navrátil, Phys. Rev. Lett. **107**, 072501 (2011).
- [3] G. Hagen, T. Papenbrock, D.J. Dean and M. Hjorth-Jensen, Phys. Rev. Lett. **101**, 092502 (2008); G. Hagen, M. Hjorth-Jensen, G.R. Jansen, R. Machleidt and T. Papenbrock, Phys. Rev. Lett. **109**, 032502 (2012).
- [4] H. Nakada, Phys. Rev. C **68**, 014316 (2003).
- [5] H. Nakada, Phys. Rev. C **78**, 054301 (2008); *ibid.* **82**, 029902(E) (2010).
- [6] G. Bertsch, J. Borysowicz, H. McManus and W.G. Love, Nucl. Phys. A **284**, 399 (1977).
- [7] N. Anantaraman, H. Toki and G.F. Bertsch, Nucl. Phys. A **398**, 269 (1983).
- [8] H. Nakada and M. Sato, Nucl. Phys. A **699**, 511 (2002); *ibid.* **714**, 696 (2003).
- [9] H. Nakada, Nucl. Phys. A **764**, 117 (2006); *ibid.* **801**, 169 (2008).
- [10] H. Nakada, Nucl. Phys. A **808**, 47 (2008).
- [11] H. Nakada, K. Mizuyama, M. Yamagami and M. Matsuo, Nucl. Phys. A **828**, 283 (2009).
- [12] H. Nakada, *Proceedings of the International Symposium "A New Era of Nuclear Structure Physics*, edited by Y. Suzuki, M. Matsuo, S. Ohya and T. Ohtsubo, p. 184 (World Scientific, Singapore, 2004).
- [13] H. Nakada, Eur. Phys. J. A **42**, 565 (2009).
- [14] H. Nakada, Phys. Rev. C **81**, 051302(R) (2010).
- [15] T. Shizuma *et al.*, Phys. Rev. C **78**, 061303(R) (2008).
- [16] T. Otsuka *et al.*, Phys. Rev. Lett. **87**, 082502 (2001).
- [17] T. Otsuka, T. Suzuki, R. Fujimoto, H. Grawe and Y. Akaishi, Phys. Rev. Lett. **95**, 232502 (2005).
- [18] H. Nakada, Phys. Rev. C **81**, 027301 (2010); *ibid.* **82**, 029903(E) (2010).
- [19] D.T. Khoa, private communication.
- [20] D.T. Loan, N.H. Tan, D.T. Khoa and J. Margueron, Phys. Rev. C **83**, 065809 (2011).
- [21] J.M. Lattimer and M. Prakash, Phys. Rep. **442**, 109 (2007).
- [22] A. Ono, P. Danielewicz, W.A. Friedman, W.G. Lynch and M.B. Tsang, Phys. Rev. C **68**, 051601(R) (2003).
- [23] A. Klimkiewicz *et al.*, Phys. Rev. C **76**, 051603(R) (2007); A. Carbone *et al.*, Phys. Rev. C **81**, 041301(R) (2010).
- [24] H.S. Than, D.T. Khoa and N.V. Giai, Phys. Rev. C **80**, 064312 (2009).
- [25] A. Akmal, V.R. Pandharipande and D.G. Ravenhall, Phys. Rev. C **58**, 1804 (1998).
- [26] B. Friedman and V.R. Pandharipande, Nucl. Phys. A **361**, 502 (1981).
- [27] ParticleDataGroup, J. Phys. G **33**, 1 (2006).
- [28] K. Suzuki, R. Okamoto and H. Kumagai, Phys. Rev. C **36**, 804 (1987); S.C. Pieper and V.R. Pandharipande, Phys. Rev. Lett. **70**, 2541 (1993).
- [29] E. Chabanat, P. Bonche, P. Haensel, J. Meyer and R. Schaeffer, Nucl. Phys. A **635**, 231 (1998).
- [30] J.F. Berger, M. Girod and D. Gogny, Comp. Phys. Comm. **63**, 365 (1991).
- [31] S. Gorieli, S. Hilaire, M. Girod and S. Pèru, Phys. Rev. Lett. **102**, 242501 (2009).

- [32] R.B. Wiringa, V. Fiks and A. Fabrocini, Phys. Rev. C **38**, 1010 (1988).
- [33] S. Shlomo, M. Kolomietz and G. Colò, Eur. Phys. J. A **30**, 23 (2006).
- [34] P. Danielewicz, Nucl. Phys. A **727**, 233 (2003).
- [35] M. Kortelainen *et al.*, Phys. Rev. C **85**, 024304 (2012).
- [36] C. Mahaux, P.F. Bortignon, R.A. Broglia and C.H. Dasso, Phys. Rep. **120**, 1 (1985).
- [37] L.-G. Cao, G. Colò and H. Sagawa, Phys. Rev. C **81**, 044302 (2010).
- [38] C. Gaarde *et al.*, Nucl. Phys. A **369**, 258 (1981); T. Suzuki, Nucl. Phys. A **379**, 110 (1982); G. Bertsch, D. Cha and H. Toki, Phys. Rev. C **24**, 533 (1981); T. Suzuki and H. Sakai, Phys. Lett. B **455**, 25 (1999).
- [39] M. Anguiano, J.L. Egido and L.M. Robledo, Nucl. Phys. A **683**, 227 (2001); T. Lesinski, T. Duguet, K. Bennaceur and J. Meyer, Eur. Phys. J. A **40**, 121 (2009); H. Nakada and M. Yamagami, Phys. Rev. C **83**, 031302(R) (2011).
- [40] G.F. Bertsch *et al.*, Phys. Rev. Lett. **99**, 032502 (2007).
- [41] G. Audi and A.H. Wapstra, Nucl. Phys. A **595**, 409 (1995); G. Audi, A.H. Wapstra and C. Thibault, Nucl. Phys. A **729**, 337 (2003).
- [42] D.T. Khoa, H.S. Than and M. Grasso, Nucl. Phys. A **722**, 92c (2003).
- [43] A. Ozawa *et al.*, Nucl. Phys. A **691** (2001) 599.
- [44] G.D. Alkhazov, S.L. Belostotsky and A.A. Vorobyov, Phys. Rep. **42**, 89 (1978).
- [45] R.B. Firestone *et al.*, *Table of Isotopes*, 8th edition (John Wiley & Sons, New York, 1996).
- [46] M. Centelles, X. Roca-Maza, X. Viñas and M. Warda, Phys. Rev. Lett. **102**, 122502 (2009).
- [47] A. Tamii *et al.*, Phys. Rev. Lett. **107**, 062502 (2011).
- [48] S. Perez-Martin and L.M. Robledo, Phys. Rev. C **78**, 014304 (2008).
- [49] N. Schunck *et al.*, Phys. Rev. C **81**, 024316 (2010).
- [50] Although the set M3Y-P5' was claimed to be fitted to the even-odd mass difference in the $Z = 50$ nuclei by the fully self-consistent HFB calculations [18], inconsistency had remained in evaluation of contribution of $v^{(DD)}$ to pairing energy.
- [51] M.M. Sharma, G. Lalazissis, J. König and P. Ring, Phys. Rev. Lett. **74**, 3744 (1995).
- [52] P. Aufmuth, K. Heilig and A. Steudel, At. Data Nucl. Data Tables **37**, 455 (1987).
- [53] I. Angeli, At. Data Nucl. Data Tables **87**, 185 (2004).
- [54] P.-G. Reinhard and H. Flocard, Nucl. Phys. A **584**, 467 (1995).
- [55] R. Kanungo, I. Tanihata and A. Ozawa, Phys. Lett. B **528** (2002) 58.
- [56] J.I. Prisciandaro *et al.*, Phys. Lett. B **510**, 17 (2001).
- [57] M. Honma, T. Otsuka, B.A. Brown and T. Mizusaki, Eur. Phys. J. A **25**, s01, 499 (2005).
- [58] R. Broda *et al.*, Phys. Rev. Lett. **74**, 868 (1995).
- [59] T. Aumann, Prog. Part. Nucl. Phys. **59**, 3 (2007); S. Gales, Prog. Part. Nucl. Phys. **59**, 22 (2007); T. Motobayashi, Prog. Part. Nucl. Phys. **59**, 32 (2007).